RSC Applied Polymers

ROYAL SOCIETY OF CHEMISTRY

PAPER

View Article Online
View Journal | View Issue

Cite this: *RSC Appl. Polym.*, 2024, **2**, 196

Dynamic quenching mechanism based optical detection of carcinogenic Cr(VI) in water and on economical paper test strips *via* a conjugated polymer†

Arvin Sain Tanwar, [a,b] Moirangthem Anita Chanu,[a] Retwik Parui, [a] Debika Barman, [a] Yeon-Ho Im*[b] and Parameswar Krishnan Iyer *[a,c]

Received 8th October 2023,
Accepted 15th October 2023

DOI: 10.1039/d3lp00195d

rsc.li/rscapplpolym

Water pollution caused by heavy metal ions and their oxo-anions comprise the biggest threats to living beings and remains a critical environmental issue. Among various water hazards, hexavalent Cr(VI) is one of the widely spread water pollutants that causes cancer. Herein, we report a very sensitive and selective conjugated polymer poly(1,1′-((2-(benzo[*c*][1,2,5]thiadiazol-4-yl)-9*H*-fluorene-9,9-diyl)bis(hexane-6,1-diyl))bis(pyridin-1-ium)dibromide) (PFPy) based sensing platform for highly accessible and quick identification of hexavalent Cr(VI) in water medium as well as on economical portable paper test strips. PFPy displayed a fluorescence "turn-off" signal in the presence of Cr(VI) *via* a dynamic fluorescence quenching mechanism with a high quenching constant of 2.25×10^5 M and a low limit of detection (LOD) *i.e.* 6.79 ppb, which is much lower than the safety limit suggested by the World Health Organization (WHO). Additionally, this analytical method was effectively used for the detection of Cr(VI) in real environmental water samples, which is desirable and challenging.

Introduction

Environmental water pollution has always been a matter of concern, and with increasing industrialization, the increase in water pollution cases has attracted great attention from researchers.[1] One of the most prevalent water hazards is toxic heavy metals and their oxo-anion species.[2] Among them, chromium (Cr) is one of the most widely used heavy metal pollutants, which usually exists in two oxidation states namely Cr(III) and Cr(VI).[3] Hexavalent Cr(VI) is highly toxic as compared to Cr(III) and is released into the environment by many industries such as tannery, electroplating, dyeing, chromate production, wood preservation, *etc.*[1] Thus it easily contaminates the adjacent natural water resources and soil, and affects the lives of living beings by entering the food chain.[4] It is classified as a Class I carcinogen that also possesses mutagenic activity.[5] Therefore, the World Health Organization (WHO) has set a maximum limit of 50 ppb of chromium in drinking water.[6] Hence, developing a sensor that can detect Cr(VI) traces in different water bodies is highly desirable and crucial. In this regard, a few analytical methods based on various techniques have been reported for monitoring the traces of Cr(VI) such as surface-enhanced Raman spectroscopy (SERS),[7,8] atomic spectroscopy,[9] electrochemical methods,[10,11] high-performance liquid chromatography-inductively coupled plasma mass spectrometry (HPLC-ICP-MS),[12] photo-electrochemical methods, *etc.*;[13] however, most of them suffer from the need for a sophisticated instrument, high cost of analysis, time-consuming processing, and lack of portability. Fluorescence-based sensors overcome these challenges and make the sensing process highly accessible, rapid, economical, portable, selective, and sensitive. Consequently, in recent times, a few fluorescent sensors have been reported for Cr(VI) sensing which include metal–organic frameworks (MOFs),[14–17] carbon dots,[18] gold nanoclusters,[19] quantum dots,[20,21] nanocomposites,[22,23] microbeads,[24] small organic molecules,[25] non-conjugated and conjugated polymers, *etc.*[26–28]

Among various applied research based on conjugated polymers (CPs),[29] their sensory applications have shown predominant potential in designing versatile sensing platforms.[30] It is their "molecular wire effect" that provides them with amplified sensing signals leading to ultra-sensitive responses.[31] The molecular wire effect is a key feature of these CPs that can

[a]*Department of Chemistry, Indian Institute of Technology Guwahati, Guwahati 781 039, India*
[b]*School of Semiconductor and Chemical Engineering, Clean Energy Research Center, Jeonbuk National University, Jeonju, Jeonbuk 54896, Republic of Korea*
[c]*Centre of Nanotechnology, Indian Institute of Technology Guwahati, Guwahati 781 039, India. E-mail: pki@iitg.ac.in, yeonhoim@jbnu.ac.kr; Fax: +913612582349*
†Electronic supplementary information (ESI) available: Experimental details, spectroscopy data, *etc.* See DOI: https://doi.org/10.1039/d3lp00195d

detect even a small perturbation in their surroundings through the alternating conjugated pi bonds in their conjugated backbone.[31] However, this amplified sensing is lacking in other non-conjugated systems. Therefore, newer CP systems have been utilized for the detection of several vital analytes.[30,32–34] The freedom of tuning or functionalization of side chains further advances their sensing capabilities.[35] The side chain can tune its solubility from a non-polar to a polar solvent and can also behave as a receptor to a distinct analyte such as Cr(VI) in the present case. Yet, interestingly, there are not many reports on CP sensors for Cr(VI) detection.[27] However, the existing sensing report is not in a 100% water medium and is also dependent on other reagents such as EDTA to achieve selectivity. Additionally, the sensitive detection of Cr(VI) on economical portable paper strips remains very challenging.[27,36] In addition, most of the reports lack a clear mechanism of sensing in the case of CPs. However, a few photophysical mechanisms have been explored in non-conjugated systems such as static quenching, the inner filter effect, photoinduced electron transfer, energy transfer, *etc.* There are also other physical phenomena based on the proximity interaction and chemical reactions such as ion exchange and redox reaction,[37] respectively, which lead to optical sensing of Cr(VI) through either of the photophysical mechanisms mentioned above.[38] Thus, keeping in view all these issues, we report highly accessible selective detection of Cr(VI) at ppb levels *via* the fluorescent CP PFPy in water as well as on economical paper test strips. Highly fluorescent PFPy showed outstanding Cr(VI) sensing at ppb levels even lower than the limit suggested by the WHO.[6] Interestingly, the mechanism of sensing was found to be a dynamic quenching mechanism, which is rare for the detection of Cr(VI) (Table 1). Thus, PFPy can be successfully utilized to detect Cr(VI) in real environmental water samples. Also, PFPy can be a good economical sensor to detect Cr(VI) in drinking water in rural areas.

Experimental section

Materials and methods

Potassium dichromate (as the Cr(VI) source) was obtained from RANKEM and used as received. All other metal salts were purchased from Sigma-Aldrich Chemicals preferably with a common counter anion such as perchlorate. Similarly, anions were preferably selected with a common counter cation such as tetrabutylammonium, if available otherwise with their most common counter cations. The entire sensing study was carried out using Milli-Q water. HPLC grade DMSO was used to prepare a stock solution of the CP PFPy (1 mM). Milli-Q water was used to prepare stock solutions of all the analytes (10 mM). A Bruker Ascend 600 spectrometer was used for recording ^{1}H NMR spectra. UV-vis experimental studies were performed on a PerkinElmer Lambda-25 spectrophotometer. Photoluminescence (PL) or fluorescence experimental studies

Table 1 A comparative study of a few sensing probes recently developed for the optical detection of Cr(VI)

Material used	Detection limit	Sensing mechanism	Test strip	Quenching constant (M^{-1})	Ref.
Conjugated polymer (PFPy)	**23.1×10^{-9} M (6.79 ppb)**	**Dynamic quenching**	**Paper based**	**2.25×10^{5}**	**This work**
TMB	0.1×10^{-6} M	Colorimetric	No	—	42
Cal-CS/PEG/Ag nanohybrids	79×10^{-9} M	Colorimetric	No	—	43
Nanoparticles	0.03×10^{-6} M	Colorimetric	Agarose based	—	44
Acridine-diphenylacetyl moiety (NDA)	0.160×10^{-6} M	Complexation ("ICT OFF")	No	—	25
MOFs	18×10^{-9} M	IFE	No	—	14
MOFs	20×10^{-9} M	Electron transfer	No	—	16
Nanocomposites	66×10^{-9} M	PET	PVDF-HFP membrane based	2.99×10^{5}	22
Carbon dots	21.1×10^{-9} M	Static quenching and IFE	PVA based	—	45
Carbon dot-wrapped Boehmite nanoparticles	58×10^{-9} M	PET	No	1.75×10^{5}	46
CB[6]-based supramolecular assembly	3.9×10^{-6} M	FRET	No	6×10^{3}	47
Gold nanoclusters	0.12×10^{-6} M	—	Paper based	13.28 ppm^{-1}	19
MOF	0.41×10^{-6} M	Absorbance of excitation light (pIFE)	No	1.38×10^{4}	48
Non-conjugated polymer (GCPF)	0.22×10^{-6} M	Oxidative damage to (GCPF)	No	—	26
Carbon dots	0.26×10^{-6} M	Static quenching	No	—	49
Carbon dots	0.4×10^{-6} M	IFE	No	—	50
Carbon quantum dots	0.14×10^{-6} M	Ionic interactions	No	—	20
Nanocomposites	1 ppb	Electron transfer	No	—	51
MOFs	3.53×10^{-6} M	Electronic interactions	No	2.07×10^{4}	52
MOFs	—	—	No	9.19×10^{5}	53
Carbon dots	1.17×10^{-6} M	IFE	No	—	54
Conjugated polymer (PFOCS)	0.072×10^{-9} M	—	No	—	27
Conjugated polymers P(Fmoc-Arg-OH), and P(Fmoc-Glu-OH)	0.016×10^{-9} M and 3.33×10^{-6} M	—	No	—	36

were performed on a Horiba Fluoromax-4 spectrofluorometer. Quartz cuvettes of 1 cm × 1 cm dimensions were used throughout the experiments. An Edinburg Life Spec II instrument was used for obtaining time-resolved photoluminescence (TRPL) spectra. Whatman paper (grade I) was used for the test strip studies.

Synthesis of the conjugated polymer (PFPy)

The CP PFPy was synthesized according to our previously established method, and was used for TNT detection at pH 12.[39] In a 10 mL RBF, the precursor polymer PF (0.095 mmol, 1 eq.) and pyridine (0.958 mmol, 10 eq.) were added to dry DMF and stirred at 70 °C under an inert atmosphere for 24 hours. Then the reaction mixture was poured into the ether and stirred to obtain precipitates, followed by washing multiple times with DCM. Thereafter the collected precipitates were dried to obtain a yellowish-orange colored product (yield = 80%) (Scheme S1†). ^{1}H NMR (600 MHz, DMSO-d_6, δ): 0.61 (b), 1.04 (b), 1.08 (b), 1.70 (b), 2.08 (b), 4.46 (b), 7.37 (b), 7.48 (b), 7.57 (b), 7.75 (b), 7.87 (b), 8.09 (b), 8.54 (b), 8.97 (b) (Fig. S1†).

TRPL studies

TRPL studies of the CP PFPy were done in water under pulse excitation at 445 nm and emission at 550 nm. Similar studies were carried out after the addition of different concentrations of Cr(VI) (Table S1†).

Portable strips

Whatman filter paper (Grade I) was used to make portable paper test strips. For this purpose, the paper was cut into a suitable size and round shape using a paper punching machine and then immersed in PFPy solution. These coated paper strips were further dried and could be later used for direct on-site detection.

PL quantum yield (Φ_s)

The absolute fluorescence quantum yield was obtained with a Horiba Fluoromax4 fluorescence spectrometer using the integrated sphere method.

LOD calculations

To evaluate the LOD, the fluorescence spectra of different solutions of PFPy (6.66 μM) in the presence of various amounts of Cr(VI) (0.0 μM, 0.033 μM, 0.066 μM, 0.100 μM, and 0.133 μM) were recorded. A calibration plot was obtained using their emission maxima and the Cr(VI) concentrations, which resulted in a linear regression equation. The LOD was evaluated using $3\sigma/k$, where k represents the slope of the aforementioned LOD plot and σ denotes the standard deviation in the emission peak of PFPy without Cr(VI).

Resonance energy transfer (RET) parameters

These were evaluated using the below-mentioned equations.[40]

$$J(\lambda) = \int_0^\infty F_D(\lambda)\varepsilon_A(\lambda)\lambda^4 d\lambda$$

where $J(\lambda)$ denotes the overlap integral, $F_D(\lambda)$ denotes the corrected fluorescence intensity of PFPy from λ to $\Delta\lambda$ with the total intensity normalized to unity, and ε_A is the molar extinction coefficient of the acceptor at wavelength λ in M^{-1} cm^{-1}.

$$R_0 = 0.211[(J)Q(\eta^{-4})(k^2)]^{1/6}$$

where R_0 denotes the Förster distance, Q represents the fluorescence quantum yield of PFPy, k^2 represents the dipole orientation factor (~0.667), and η is the refractive index of the medium.

Inner filter effect (IFE) corrections

These corrections were done using the below-mentioned equation.[41]

$$I_{corr}/I_{obs} = 10^{(A_{ex}+A_{em})/2}$$

where I_{obs} and I_{corr} are the fluorescence emissions before and after IFE correction, respectively, and A_{ex} and A_{em} are the absorbances of the samples at excitation and emission wavelengths, respectively.

Results and discussion

Photophysical studies of PFPy

The CP PFPy (Fig. 1a) structurally resembles the family of ionic conjugated polymers or conjugated polyelectrolytes and was synthesized using our previously established post-polymerization functionalization method.[39] Side chain terminals of PFPy contain cationic pyridinium, which enhances its solubility in polar solvents and behaves as a receptor unit for negatively charged species such as oxo-anionic species of Cr(VI) due to favorable ionic attractions *via* ion-exchange (Fig. 1a).[38] The cationic CP PFPy is highly fluorescent in water with a PL quantum yield of 0.59. PFPy shows absorption and fluorescence at 430 nm and 552 nm (430 nm excitation), respectively, in aqueous medium (Fig. S2†). All the sensing experiments were performed in an aqueous medium and the results were analysed.

Sensing studies

To investigate the sensing behavior of the CP PFPy towards Cr(VI), PL titrations were performed by gradually increasing the concentration of Cr(VI) in an aqueous solution of highly fluorescent PFPy (Fig. 1b). Initially, after the addition of a very dilute solution of Cr(VI) (0.33 μM), there was immediate ~10% quenching in the PL spectra of PFPy, while the concentration of Cr(VI) was further increased and the PL intensity of PFPy further quenched to ~82% (Fig. 1b). This fading of the yellow fluorescence of PFPy in the presence of Cr(VI) can also be

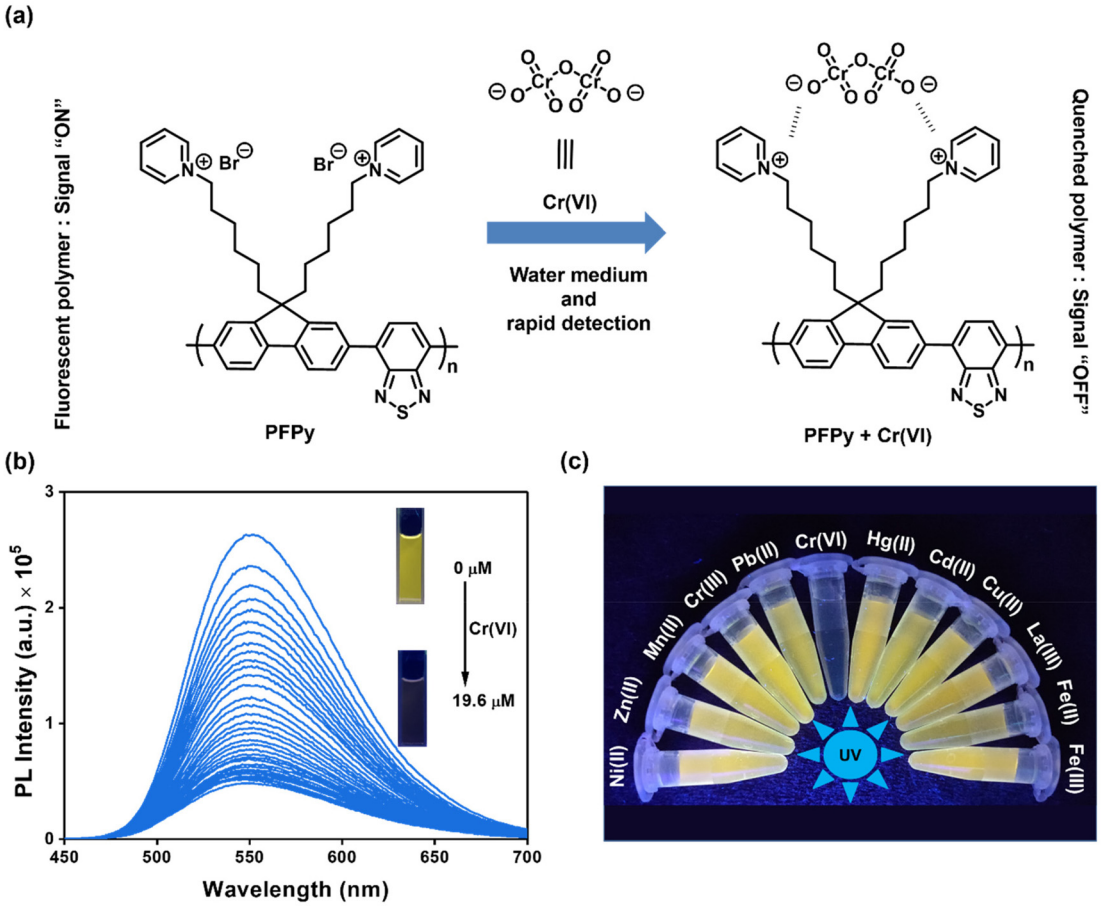

Fig. 1 (a) Chemical structure of PFPy and illustration of Cr(VI) sensing under an excitation light source; (b) fluorescence spectra of PFPy (6.66 μM) with an increase in the concentration of Cr(VI) (inset: images of the PFPy solution before and after addition of Cr(VI)); (c) photograph of PFPy solution in the presence of various analytes (20.0 μM) in water under a UV lamp of 365 nm excitation wavelength.

observed under a UV lamp (Fig. 1b (inset)). These results suggest that PFPy is highly sensitive to Cr(VI) and thus a low LOD value was obtained for Cr(VI) *i.e.* 23.1 nm (~6.79 ppb) (Fig. S3†), which is comparable with the literature for Cr(VI) detection in aqueous medium (Table 1).

Selectivity studies

Sensitivity and selectivity are two important criteria for any sensing system that help in determining the best sensor platform. Therefore, to check the selectivity of the CP PFPy for Cr (VI), various other interfering metal ions such as Cr(III), Cu(II), Cd(II), Fe(II), Fe(III), Hg(II), La(III), Mn(II), NI(II), Pb(II), and Zn(II), and inorganic anions such as BF_4^-, $H_2PO_4^-$, HPO_4^{2-}, N_3^-, CO_3^{2-}, NO_3^-, and PO_4^{3-} were tested under the same experimental setup. It was found that these analytes did not have any substantial influence on the PL intensity of the CP PFPy, which can be seen in Fig. 1c, 2a, S4, and S5.† This extraordinary selectivity for Cr(VI) exhibited by PFPy can also be seen in the Stern–Volmer 3D plots (Fig. 2b), where the quenching efficiency of all the metal ions is insignificant in comparison with the quenching efficiency of Cr(VI). Furthermore, selectivity studies in the presence of a competitive environment were also carried out. As the Cr(VI) undergoes redox reactions and may have some interference in the presence of other redox active ions or molecules. Moreover, there may be some electrolyte effects of other ions in selective detection. In this regard, first the PL spectrum of PFPy was obtained and then Cr(III) ions were added; this would allow Cr(III) ions to interact with PFPy and create a competitive environment for Cr(VI) prior to its addition finally. It was noticed that the addition of Cr(III) caused a trivial change in the PL spectra of PFPy, while the addition of Cr(VI) significantly quenched the PL spectra of PFPy even in the presence of an interfering environment (Fig. 2c). Similarly, selectivity studies were carried out in a competitive environment of remaining metal ions as well as anions and not very different results were obtained (Fig. 2c and S6–S23†). We further studied the effect of other oxoanions such as permanganate, arsenate, *etc.*, and some electrolyte solutions such as $MgSO_4$, KIO_3, $NaNO_3$ and $NaHCO_3$, which are easily available, and compared their responses with PFPy. It was observed that oxyanions such as arsenate and arsenite having negative charges could not cause any significant change in the PL signal (Fig. S24†). However, little quenching was observed in the case of permanganate, and still the maximum response

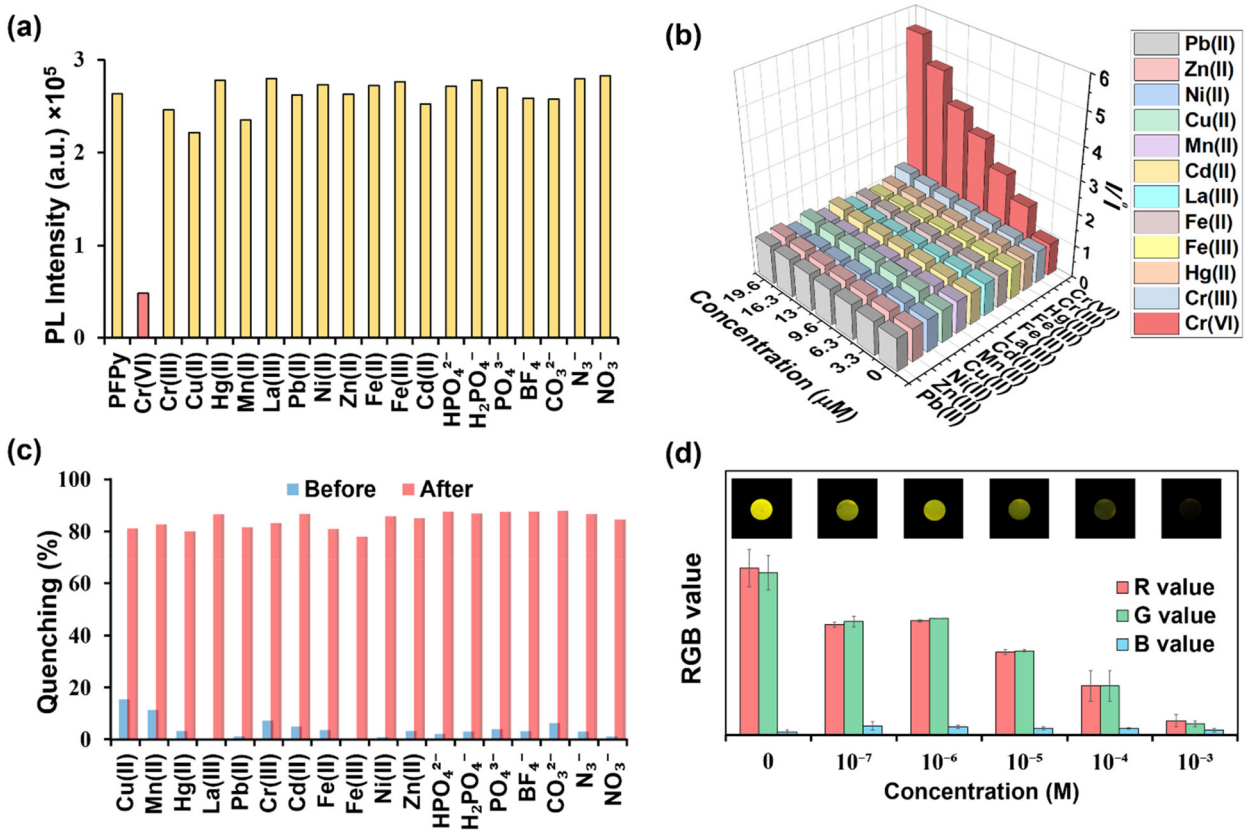

Fig. 2 (a) Effect of various analytes (cations and anions) on the PL intensity of PFPy (6.66 μM); (b) 3D-Stern–Volmer plots for all the metal ions; (c) quenching (%) of PFPy with various analytes in water before and after addition of Cr(VI); (d) sensing on portable economical paper strips: images depict the round fluorescent test strip after dipping in various solutions of different concentrations of Cr(VI) under a UV irradiating hand-lamp of 365 nm wavelength, and their respective RGB analysis.

was obtained for Cr(VI) (Fig. S24†). Moreover, the electrolyte solutions could not quench the emission of PFPy and a similar response was obtained for Cr(VI) (Fig. S25†). This can be understood that among them Cr(VI) possesses the highest quenching efficiency which might have more interaction with the excited state PFPy through the dynamic quenching mechanism. Overall, these experiments confirm that PFPy has remarkable sensitivity and exceptional selectivity towards Cr(VI) even in the presence of various ions and can be a reliable sensing system for real environmental monitoring.

Detection of Cr(VI) on sensing strips

Considering the cost of the sensing platform and its feasibility for on-site detection in remote areas, portable sensing strips were developed. For this purpose, Whatman filter paper (Grade I) was taken and cut into desirable round shapes using a paper punching machine with a hole diameter of around 0.25 inches. After that, these strips were first coated with PFPy and subsequently dried in air for the direct application of on-site Cr(VI) sensing. Later these strips were dipped in water samples containing different concentrations of Cr(VI) and then dried before taking photographs under UV light (excitation = 365 nm). As a result, quenching of fluorescence was observed on the highly fluorescent PFPy-coated paper strip under a UV lamp (Fig. 2d). The quenching of the fluorescent test paper strip increases with the increase in the concentration of Cr(VI) in water. This fluorescence quenching on the sensing strip can be quantitatively analyzed using RGB values obtained using ZEN 3.6 (blue edition) software. It was found that the RG values decrease with the increase in the concentration of Cr(VI) indicating fluorescence quenching (Fig. 2d). These strips are highly sensitive, which can be realized from Fig. S26 and S27;† however, to obtain a linear calibrated plot, a graph of logarithm of concentration *vs.* RG values was plotted. A good linear fitting was achieved up to 10^{-7} M with $R^2 > 0.9$ (Fig. S26 and S27†). These results suggest that the practical utility of this analytical method can be extended to natural water samples.

Mechanism of sensing

Recently fluorescence-based sensing mechanisms have been well explored in a step-by-step series of simple experiments.[35] To analyze the mechanism of sensing, a detailed Stern–Volmer plot was obtained first, from which it was found to be the best fit for a linear regression line ($Y = a + bX$) (Fig. 3a). This linear regression equation of line indicated that fluorescence quenching occurs either due to the dynamic or static fluo-

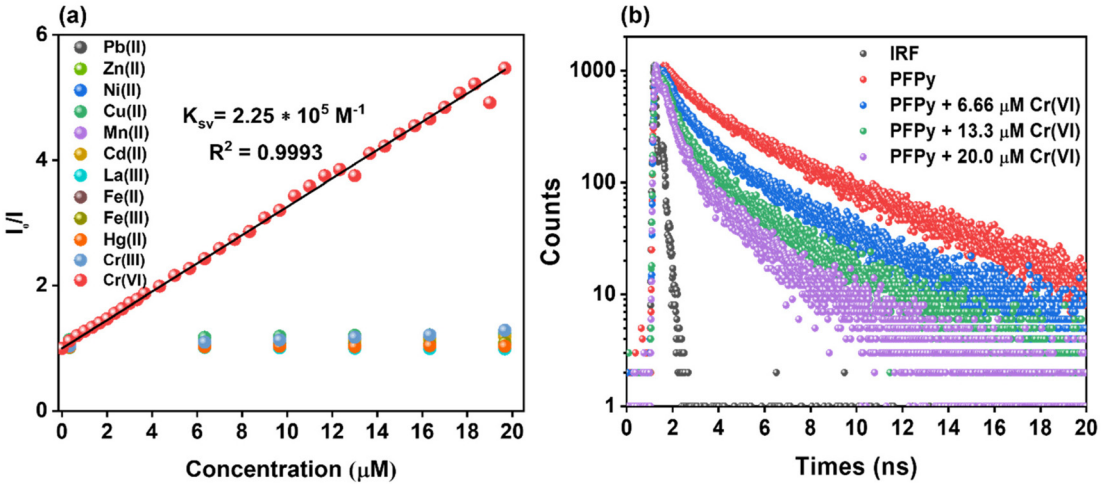

Fig. 3 (a) Determination of the Stern–Volmer constant (K_{SV}) for Cr(VI) in water, and 2D S–V plots for various metal ions; (b) TRPL spectra of PFPy (6.66 μM) with different concentrations of Cr(VI) (6.66, 13.3 and 20.0 μM) in water, where IRF denotes the "Instrument Response Function".

rescence quenching mechanism. In this equation (Fig. 3a), "*Y*" represents the ratio of PL intensity of PFPy before and after the addition of Cr(VI) *i.e.* I_o/I, "*a*" is the intercept whose value is 1, and the slope of this equation represents the Stern–Volmer constant (K_{SV}), which was found to be 2.25 × 10^5 M^{-1}. This remarkably high value of K_{SV} signifies the high efficiency of fluorescence quenching for Cr(VI) and when compared with other analytes also suggests high selectivity towards Cr(VI) (Fig. 3a).

Furthermore, the role of the dynamic type of fluorescence quenching in the sensing mechanism, which may include collisional interactions of the fluorophore (PFPy) with a quencher (Cr(VI)) or an excited state process such as RET, in which the excited fluorophore emits energy that is absorbed by the nearby quencher molecules, was also analyzed carefully. To verify this, TRPL experiments of PFPy were carried out in the absence and presence of different amounts of quencher [Cr (VI)] (Fig. 3b), and the corresponding fluorescence lifetime decay of PFPy was examined. Interestingly, the fluorescence lifetime of PFPy (3.96 ns) gradually reduced to 1.53 ns after the addition of Cr(VI) (Table S1†). This decrement in the fluorescence lifetime with an increase in the concentration of the quencher [Cr(VI)] confirms the involvement of dynamic quenching in the sensing process (Table S1†).[40]

Since dynamic quenching occurs in the sensing process, the possibility of RET occurrence was investigated. RET is governed by three factors; first, the spectral overlap factor between the quencher (absorbance spectrum) and the fluorophore (emission spectrum), second, the distance between them, and third, their dipole orientation. For this purpose, initially, a spectral overlap was plotted between the emission spectrum of PFPy with the absorbance spectrum of Cr(VI) (Fig. 4a). A spectral overlap was observed from 440 nm to 523 nm and the corresponding overlap integral $J(\lambda)$ was calculated and found to be 1.92 × 10^{11} M^{-1} cm^{-1} nm^4 (Table S2†). Förster distance (R_0) was also calculated and was found to be 11.32 Å, which is also favorable for an effective RET process (Table S2†). Also, the RET efficiency was evaluated using this formula and found to be 61.63%. Hence all these factors confirmed the involvement of the RET process in the sensing mechanism. Just like in RET, the spectral overlap also plays a key role in sensing based on the inner filter effect (IFE) mechanism, where spectral overlap between emission and/or excitation spectra of the fluorophore (PFPy) is overlapped with the absorption spectrum of the quencher (Cr(VI)) (Fig. 4a). This can be corrected and confirmed using IFE corrections. It can be seen in Fig. 4b that there is not a major change in PL intensities after IFE correction. Also, almost negligible change was observed in suppression efficiencies (Fig. 4b, Table S3†). Thus, it can be concluded that IFE does not play any key role in the sensing process.

Furthermore, to investigate the role of static quenching in the sensing process, the absorption spectra of PFPy and Cr(VI) were compared with that of a mixed solution of both *i.e.* PFPy + Cr(VI) (Fig. 4c). It was found that there is no major shift in absorption peak in PFPy after the addition of Cr(VI), except for a minor increment in the absorption value. Moreover, the new peak appearing in the mixture resembles the Cr(VI) peak only (Fig. 4c). Thus, it can be concluded that static quenching does not have any key involvement in the sensing process. Based on all the above observations, it can be concluded that sensing of Cr(VI) by PFPy takes place exclusively due to the dynamic type of quenching mechanism (Fig. 4d), which is very rare in the case of Cr(VI) (Table 1). The dynamic quenching mechanism is a phenomenon observed in phosphorescence and fluorescence spectroscopy, where the intensity and lifetime of the emitted light are reduced due to the interaction of the fluorophore with a quencher molecule.[55] Quenching occurs through a collision or close approach between the excited state fluorophore and the quencher. The excited fluorophore can transfer its energy to the quencher through various processes *viz.* collisional quenching, energy transfer, electron transfer, *etc.* All these processes lead to quenching *via* dynamic quenching

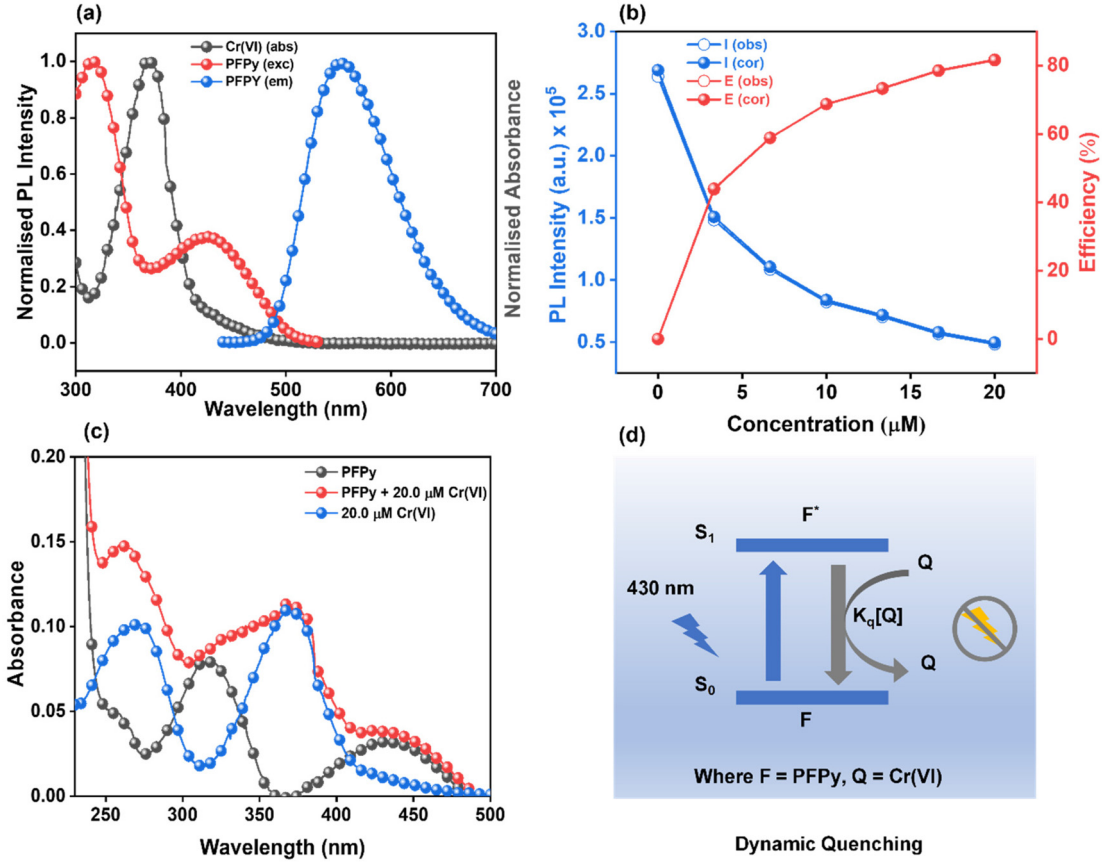

Fig. 4 (a) Spectral overlap between the excitation and emission spectra (normalized) of PFPy with the absorption spectrum (normalized) of Cr(VI); (b) PL intensity of PFPy (6.66 μM) before and after IFE correction at various concentrations of Cr(VI), and the percentage quenching efficiency ($E\% = 1 - I/I_0$) of the observed and corrected measurements of PFPy at various concentrations of Cr(VI); (c) absorbance spectra of PFPy (6.66 μM) with and without Cr(VI) (20.0 μM), and only Cr(VI) (20.0 μM) without PFPy; (d) illustration of the dynamic quenching mechanism for the detection of Cr(VI), where *Q* denotes a quencher *i.e.* Cr(VI) and *F* denotes a fluorophore *i.e.* PFPy.

mechanisms, which results through the interaction of the excited state fluorophore and quencher molecules.[55] In the present case, a similar interaction was observed between the excited state of PFPy and the Cr(VI) that leads to the quenching of the emitted light of PFPy along with a reduction in the lifetime of emitted light of PFPy due to the close interaction of the excited state of PFPy and Cr(VI) (Fig. 3b). Additionally, the extent of energy transfer was also evaluated which further confirms the dynamic quenching mechanism (Table S2†).

Table 2 Detection of Cr(VI) in environment samples

Sample	Added (μM)	Found[a] (μM)	Recovery (%)
Lake water	0.80	0.76 ± 7.02	95.0
	2.00	1.80 ± 1.64	90.0
	10.00	9.63 ± 3.51	96.3

[a] An average of three replicate measurements.

Cr(VI) sensing in environmental samples

For any sensing system, its applicability to the detection of pollutants in natural water samples is highly desirable. For this purpose, the PFPy sensor was tested for Cr(VI) using a natural water reservoir. Various water samples were collected from nearby resources such as "Serpentine Lake" water, IITG. Before testing, these samples were filtered through membranes (0.2 μm in pore size) and then directly used for testing. These samples did not significantly affect the PL intensity of PFPy, confirming the absence of Cr(VI). Therefore, these samples were spiked with known concentrations of Cr(VI) and then examined using the same set of experiments (Table 2). When compared with the calibration plot obtained for Cr(VI) (Fig. S28†), these spiked samples displayed high values of recoveries with a relative standard deviation (RSD) of less than 8% (Fig. S29†). These results further suggest that PFPy may be a reliable sensor for sensing Cr(VI) at real environmental sites. Furthermore, these Cr(VI) spiked lake water samples were also tested using economical paper test strips. Fig. 5 shows images of these paper strips after exposure to various amounts of Cr (VI) in lake water, and their corresponding RG analysis which quite matches the RG values obtained in the case of a standard solution of Cr(VI) in Milli-Q water. Thus, this analytical method

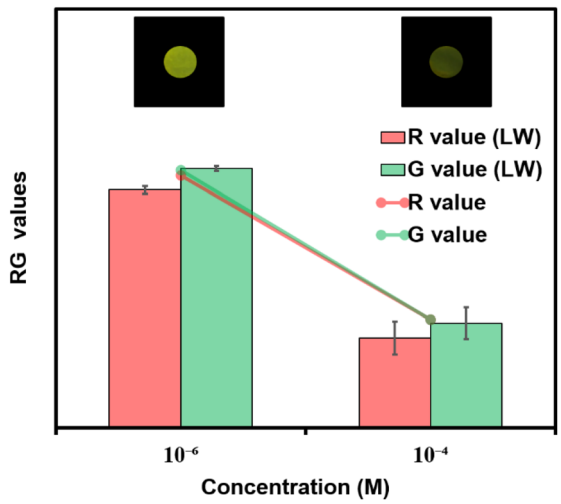

Fig. 5 Sensing on portable paper strips; images depict the fluorescent test strip after dipping in various samples of lake water (LW) spiked with different concentrations of Cr(VI) under a UV irradiating hand-lamp of 365 nm wavelength, and their respective RG analysis and comparison with the standard paper strip RG values.

can be a reliable, highly accessible, and economical method for the on-site detection of Cr(VI).

Conclusions

In summary, an easily accessible and rapid fluorescence-based analytical method for the detection of carcinogenic hexavalent Cr(VI) in water and on portable solid platforms is successfully developed. This analytical method is comprised of a highly fluorescent cationic conjugated polymer PFPy that can detect remarkably up to 6.79 ppb levels of Cr(VI) in water with a quenching constant of 2.25×10^5 M^{-1}. PFPy displays extraordinary selectivity for Cr(VI) even in a highly competitive environment of other interfering ions. The unprecedented results in terms of ultra-sensitivity and remarkable selectivity were realized due to the dynamic fluorescence quenching mechanism, which is rarely observed in the case of Cr(VI). Furthermore, the economical and portable paper test strips were successfully developed which can distinguish various solutions of Cr(VI) from 10^{-7} to 10^{-3} M, and even work well in lake water, making them a simple, cost-effective, and reliable sensor for real environmental water pollution.

Conflicts of interest

There are no conflicts to declare.

Acknowledgements

The financial assistance from the Department of Science and Technology (DST), New Delhi (No. DST/CRG/2019/002614), the DST-Max Planck Society, Germany (IGSTC/MPG/PG(PKI)/2011A/48), and the Department of Electronics & Information Technology (DeitY) No. 5(1)/2022-NANO is gratefully acknowledged. The CIF and Department of Chemistry, IIT Guwahati are acknowledged for instrument facilities.

References

1 N. Gysi and A. Bernhardt, *World's Worst Pollution Problems*, 2016.
2 S. Dutta, S. Let, M. M. Shirolkar, A. V. Desai, P. Samanta, S. Fajal, Y. D. More and S. K. Ghosh, *Dalton Trans.*, 2021, **50**, 10133–10141.
3 C. M. Stern, T. O. Jegede, V. A. Hulse and N. Elgrishi, *Chem. Soc. Rev.*, 2021, **50**, 1642–1667.
4 M. Tumolo, V. Ancona, D. De Paola, D. Losacco, C. Campanale, C. Massarelli and V. F. Uricchio, *Int. J. Environ. Res. Public Health*, 2020, **17**, 5438.
5 M. Costa and C. B. Klein, *Crit. Rev. Toxicol.*, 2006, **36**, 155–163.
6 W. H. Organization, *Guidelines for drinking-water quality*, World Health Organization, 1993.
7 X. Bu, Z. Zhang, L. Zhang, P. Li, J. Wu, H. Zhang and Y. Tian, *Sens. Actuators, B*, 2018, **273**, 1519–1524.
8 Y. Long, H. Li, W. Wang, X. Yang and Z. Liu, *J. Alloys Compd.*, 2022, **910**, 164916.
9 J. Nan and X.-P. Yan, *Anal. Chim. Acta*, 2005, **536**, 207–212.
10 M. H. Motaghedifard, S. M. Pourmortazavi and S. Mirsadeghi, *Sens. Actuators, B*, 2021, **327**, 128882.
11 N. Jayaraman, Y. Palani, R. R. Jonnalagadda and E. Shanmugam, *Sens. Actuators, B*, 2022, **367**, 132165.
12 A. F. Roig-Navarro, Y. Martinez-Bravo, F. J. López and F. Hernández, *J. Chromatogr. A*, 2001, **912**, 319–327.
13 T. Fang, X. Yang, L. Zhang and J. Gong, *J. Hazard. Mater.*, 2016, **312**, 106–113.
14 L. Qiu, Z. Ma, P. Li, X. Hu, C. Chen, X. Zhu, M. Liu, Y. Zhang, H. Li and S. Yao, *J. Hazard. Mater.*, 2021, **419**, 126443.
15 Y. Zhang, Y. Liu, F. Huo, B. Zhang, W. Su and X. Yang, *ACS Appl. Nano Mater.*, 2022, **5**, 9223–9229.
16 W. Shi, M. He, W. Li, X. Wei, B. Bui, M. Chen and W. Chen, *ACS Appl. Nano Mater.*, 2021, **4**, 802–810.
17 S. C. Pal, D. Mukherjee and M. C. Das, *Inorg. Chem.*, 2022, **61**(31), 12396–12405.
18 A. Tall, F. A. Cunha, B. Kaboré, C. D. D. E. S. Barbosa, U. Rocha, T. O. Sales, M. O. F. Goulart, I. Tapsoba and J. C. C. Santos, *Microchem. J.*, 2021, **166**, 106219.
19 Y. B. Yin, C. L. Conrad, K. N. Heck, F. Lejarza and M. S. Wong, *ACS Appl. Mater. Interfaces*, 2019, **11**, 17491–17500.
20 H.-Y. Li, D. Li, Y. Guo, Y. Yang, W. Wei and B. Xie, *Sens. Actuators, B*, 2018, **277**, 30–38.
21 J. Cai, G. Han, J. Ren, C. Liu, J. Wang and X. Wang, *Chem. Eng. J.*, 2022, **435**, 131833.

22 S. Roy, S. Bardhan, D. Mondal, I. Saha, J. Roy, S. Das, D. K. Chanda, P. Karmakar and S. Das, *Sens. Actuators, B*, 2021, **348**, 130662.
23 Q. Jin, M. Dai, X. Zhan, S. Wang and Z. He, *J. Alloys Compd.*, 2022, **922**, 166268.
24 M. Li, Y. Tang, R. Zhao, T. Gao and L. Zhang, *J. Hazard. Mater.*, 2022, **433**, 128809.
25 P. Ravichandiran, D. S. Prabakaran, N. Maroli, A. R. Kim, B.-H. Park, M.-K. Han, T. Ramesh, S. Ponpandian and D. J. Yoo, *J. Hazard. Mater.*, 2021, **419**, 126409.
26 J. Song, H. Zhou, R. Gao, Y. Zhang, H. Zhang, Y. Zhang, G. Wang, P. K. Wong and H. Zhao, *ACS Sens.*, 2018, **3**, 792–798.
27 L. Zou, Y. Wen, H. Zhang, J. Chai, X. Duan, L. Shen, G. Zhang and J. Xu, *Sens. Actuators, B*, 2018, **277**, 394–400.
28 B. Li, Q.-Q. Yan and G.-P. Yong, *J. Mater. Chem. C*, 2020, **8**, 11786–11795.
29 N. Zehra, D. Dutta, A. H. Malik, S. S. Ghosh and P. K. Iyer, *ACS Appl. Mater. Interfaces*, 2018, **10**, 27603–27611.
30 S. Hussain, A. H. Malik and P. K. Iyer, *ACS Appl. Mater. Interfaces*, 2015, **7**, 3189–3198.
31 S. W. Thomas, G. D. Joly and T. M. Swager, *Chem. Rev.*, 2007, **107**, 1339–1386.
32 N. Zehra, A. S. Tanwar, M. N. Khatun, L. R. Adil and P. K. Iyer, in *Progress in Molecular Biology and Translational Science*, ed. R. S. Bhosale and V. Singh, Academic Press, 2021, vol. 185, pp. 137–177.
33 M. A. Chanu, S. Mondal, N. Zehra, A. S. Tanwar and P. K. Iyer, *ACS Appl. Polym. Mater.*, 2022, **4**, 3491–3497.
34 A. S. Tanwar, M. Mehtab, J.-T. Kim, K.-J. Oh, P. K. Iyer and Y.-H. Im, *Chem. Eng. J.*, 2023, **456**, 141002.
35 A. S. Tanwar, N. Meher, L. R. Adil and P. K. Iyer, *Analyst*, 2020, **145**, 4753–4767.
36 F. Li, G. Zhang, L. Zou, X. Zhang, F. Liu, H. Li, J. Xu and X. Duan, *ACS Appl. Polym. Mater.*, 2022, **4**, 815–821.
37 S. Wang, W. Guo, Y. Liu, X. Ma, L. Zhang, H. Hao, X. Shi, H. Yan, X. Kong, J. Yin, H. Zhou, X. Li, L. Kong, G. Chen, X. Ju, Y. Yang, H. Zhu, Y. Li and F. Dai, *Cryst. Growth Des.*, 2023, **23**, 4115–4129.
38 S. Yadav, N. Choudhary, S. Bhai, G. Bhojani, S. Chatterjee, B. Ganguly and A. R. Paital, *ACS Appl. Bio Mater.*, 2021, **4**, 6430–6440.
39 A. S. Tanwar, R. Parui, R. Garai, M. A. Chanu and P. K. Iyer, *ACS Meas. Sci. Au*, 2022, **2**, 23–30.
40 A. S. Tanwar, L. R. Adil, M. A. Afroz and P. K. Iyer, *ACS Sens.*, 2018, **3**, 1451–1461.
41 A. S. Tanwar, S. Patidar, S. Ahirwar, S. Dehingia and P. K. Iyer, *Analyst*, 2019, **144**, 669–676.
42 J. Liao, Y. Wu, X. Chen, H. Yu, Y. Lin, K. Huang, J. Zhang and C. Zheng, *J. Hazard. Mater.*, 2022, **440**, 129812.
43 M. Liu, S. Zhang, Y. Wang, J. Liu, W. Hu and X. Lu, *Anal. Chem.*, 2022, **94**, 1669–1677.
44 S. Bhatt, G. Vyas and P. Paul, *ACS Omega*, 2022, **7**, 1318–1328.
45 Y. Ji, X. Zou, W. Wang, T. Wang, S. Zhang and Z. Gong, *Microchem. J.*, 2021, **167**, 106284.
46 S. Roy, S. Bardhan, D. K. Chanda, J. Roy, D. Mondal and S. Das, *ACS Appl. Mater. Interfaces*, 2020, **12**, 43833–43843.
47 J. Sun, P. Guo, M. Liu and H. Li, *J. Mater. Chem. C*, 2019, **7**, 8992–8999.
48 P. Li, X.-M. Yin, L.-L. Gao, S.-L. Yang, Q. Sui, T. Gong and E.-Q. Gao, *ACS Appl. Nano Mater.*, 2019, **2**, 4646–4654.
49 Y. Gao, Y. Jiao, W. Lu, Y. Liu, H. Han, X. Gong, M. Xian, S. Shuang and C. Dong, *J. Mater. Chem. B*, 2018, **6**, 6099–6107.
50 Y. Ma, Y. Chen, J. Liu, Y. Han, S. Ma and X. Chen, *Talanta*, 2018, **185**, 249–257.
51 X. Shen, X. Yang, C. Su, J. Yang, L. Zhang, B. Liu, S. Gao, F. Gai, Z. Shao and G. Gao, *J. Mater. Chem. C*, 2018, **6**, 2088–2094.
52 X.-Y. Guo, F. Zhao, J.-J. Liu, Z.-L. Liu and Y.-Q. Wang, *J. Mater. Chem. A*, 2017, **5**, 20035–20043.
53 B.-B. Lu, W. Jiang, J. Yang, Y.-Y. Liu and J.-F. Ma, *ACS Appl. Mater. Interfaces*, 2017, **9**, 39441–39449.
54 H.-Y. Zhang, Y. Wang, S. Xiao, H. Wang, J.-H. Wang and L. Feng, *Biosens. Bioelectron.*, 2017, **87**, 46–52.
55 J. R. Lakowicz, *Principles of fluorescence spectroscopy*, Springer, 2006.